Modeling of the Tridentate Amorphous Silica Ligand

Jean-Michel Garrot, Christine Lepetit,* and Michel Che†

Laboratoire de Réactivité de Surface, UMR 7609 CNRS, Université Pierre et Marie Curie, Tour 54-55, 2ème étage, 4, Place Jussieu, 75252 Paris Cedex 05, France

Patrick Chaquin

Laboratoire de Chimie Théorique, UMR 7616 CNRS, Université P. et M. Curie, Tour 22-23, 1er étage, 4, Place Jussieu, 75252 Paris Cedex 05, France

Received: April 10, 2001; In Final Form: July 17, 2001

The 3-fold coordination of Ni^{II} cations to amorphous silica is modeled performing density functional theory (DFT) calculations on framework model clusters of increasing size. Using the *n*T notation of zeolite structures where *n* is the number of T atoms (T = Si or Al), four model clusters with the following structures are investigated: (i) $(Si_2O_3H_4)^{2-}$ (**2T**) is made of two vicinal silanolate groups (SiO^-) bonded through an oxygen bridge. The valence requirements of silicium are satisfied by addition of terminal hydrogen atoms. (ii) $(Si_3O_6H_4)^{2-}$ (**3T**) is a six-membered ring made of two silanolate groups and one silanol group (SiOH) bonded through oxygen bridges. (iii) $(Si_4O_7H_6)^{2-}$ (**4T**) is an eight-membered ring with two vicinal silanolate groups in positions 1 and 3 and a silanol group in position 5, and (iv) $(Si_5O_8H_8)^{2-}$ (**5T**) is a flexible ten-membered ring with two vicinal silanolate groups in positions 1 and 3 and an isolated silanol group in position 7. DFT calculations are performed in order to estimate the ability of each model cluster to reproduce the experimental characteristics of previously described silica-supported $Ni^{II}(O)_3$ species: (i) three-coordinated Ni^{II} of distorted C_{3v} close to D_{3h} symmetry and (ii) Ni−O distances in agreement with EXAFS measurements. $(Si_5O_8H_8)^{2-}$ is preferred to the $(Si_2O_3H_4)^{2-}$ model proposed earlier. Because of its flexibility, the larger framework model is able to best reproduce the experimental geometry of the Ni^{II} site. This model cluster may be assimilated to two vicinal silanolates and one neighboring isolated silanol or siloxane bridge on the real silica surface.

Introduction

Oxide-supported transition metal complexes constitute a broad class of heterogeneous catalysts.[1,2] During the grafting process of the active metallic center onto the oxide support, some mobile ligands of the precursor complex are substituted by hydroxyl groups or oxide ions of the support, which are then acting as true ligands. The resulting mixed ligand complex combines the remaining ligands of the starting organometallic complex and the new supermolecular surface ligand.

A specificity of this interfacial coordination chemistry[3−5] is the possibility to completely remove the mobile ligands during a subsequent thermal treatment to retain only the ligands of the surface and to yield coordination vacancies, the reactivity of which is the driving force for molecular adsorption and catalysis inside the coordination sphere of the metallic center.

$Ni^{II}(O)_3$ complexes supported on amorphous silica, which are the precursors of ethylene or propylene dimerization catalysts,[6] have been prepared using this approach. In the first step of the preparation, nickel is introduced onto the silica support from aqueous solutions of $[Ni(en)_2(H_2O)_2]^{2+}$[7] (en = ethanediamine) or $[Ni(NH_3)_6]^{2+}$,[8,9] following previously described procedures.[7−9] Upon nickel grafting, the exchange of two water or ammonia ligands for support surface groups is evidenced.[7,9] Upon a suitable thermal treatment,[10,11] the silica support turns from a bidentate to a tridentate supermolecular ligand. Indeed, ammine ligands are completely removed, and the nickel cation remains bonded only to three oxygen atoms of the surface. The distorted C_{3v} close to D_{3h} symmetry of this highly unsaturated $Ni^{II}(O)_3$ site (which will be referred to as Ni^{II}_{3c}) is deduced from diffuse reflectance spectroscopy in the UV−visible range[8] and XANES analysis.[12] The 3-fold coordination is confirmed by EXAFS, and different Ni−O distances are measured for Ni^{II}_{3c} sites: (i) two short Ni−O bond lengths in the range of 1.74−1.76 Å and (ii) one longer Ni−O bond length in the 1.95−2.06 Å range.[13] The spectroscopic characterization of Ni^{II}_{3c} sites is summarized in Table 1.

Ni^{II}_{3c} may be photoreduced into the corresponding $Ni^{I}(O)_3$ complex.[14] Upon introduction of trialkylphosphine (TAP) in the coordination sphere of Ni^{I}, the resulting supported complexes are active for ethylene dimerization into butene[15] and propylene dimerization into hexenes;[6] the selectivity for α-olefins is related to the electronic and steric effects of the TAP ligand.[6,15]

Because of the difficult experimental characterization of amorphous silica, the local environment of Ni^{II}_{3c} remains unclear and is deduced from spectroscopic measurements which give the symmetry or Ni−O distances (Table 1). But the local structure of the coordination site at the surface as well as the precise nature of the supermolecular ligand are not well-known. Modeling studies may be helpful in order to elucidate the latter questions.

* Corresponding author. Current address: Laboratoire de Chimie de Coordination, UPR 8241 CNRS, 205 Route de Narbonne, 31077 Toulouse, France. Phone: 33 05 61 33 31 35. Fax: 33 05 61 55 30 03. E-mail: lepetit@lcc-toulouse.fr.

† Institut Universitaire de France.

10.1021/jp011329p CCC: $20.00
Published on Web 09/19/2001

TABLE 1: Experimental Characterization of Silica-sSupported Ni^{II}_{3c}

interpretation	analysis	measurements	spectroscopy	ref
three-coordinated Ni^{II}	symmetry	distorted C_{3v} or D_{3h}	diffuse reflectance spectroscopy in the UV−visible range	8
three-coordinated Ni^{II}	symmetry	C_{3v} but close to D_{3h}	XANES	12
three-coordinated Ni^{II}	two short Ni−O distances	1.74−1.76 Å	EXAFS	13
two types of Ni−O bond ↓ two types of surface ligand	one long Ni−O distance	1.95−2.06 Å	EXAFS	13
triplet state	spin state	$M = 3.9\ \mu_B$	magnetic susceptibility measurements	10

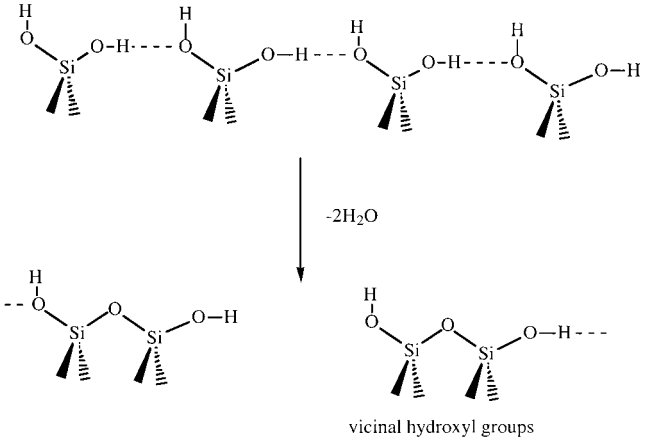

Figure 1. Dehydratation scheme of the (100) surface of β-cristobalite as proposed by Shay et al. from ref 19.

From the literature, it appears that various approaches have been used to model the surface of amorphous silica.

One possibility is based on the structure of β-cristobalite. Indeed, DRX studies of silica have shown the existence of a local order which resembles that of β-cristobalite and related crystalline phases.[16,17] The surface is heterogeneous and probably composed of regions of partially hydroxylated (100) and (111) β-cristobalite surfaces.[18] The hydroxylated (100) surface exhibits geminal hydroxyl groups $Si(OH)_2$-linked in chains through H-bonding interaction and which may yield siloxane bridges Si−O−Si upon dehydroxylation (Figure 1).[19]

On the other hand, the (111) surface is made of isolated silanol groups (SiOH) that cannot be dehydroxylated. This model has been used together with molecular mechanics relaxation to model Os and Rh clusters supported on amorphous silica.[18] Singly oxygen-bridged surface complexes (μ-H)-(μ-OSi≡) $Os_3(CO)_{10}$ are predicted to be more stable than their double oxygen-bridged analogues (μ-OSi≡)$_2$ $Os_3(CO)_{10}$.[19]

The above crystalline-type model of silica exhibits only two types of surface ligands—(i) Si−O−Si siloxane groups and (ii) isolated Si−OH silanol groups—and appears to be quite far from the real amorphous silica, which is much more heterogeneous, as shown below from molecular dynamics studies.

Indeed, vitreous silica surface models have been generated by molecular dynamics using the simulated annealing techniques.[20] A three-body potential including the dominant ionic interactions and the weak covalent character of vitreous silica was developed, and the structural features of bulk silica (average bond distances or angle distribution) were accurately reproduced in the model obtained through molecular dynamics simulations.[21] A snapshot of a silica surface obtained by molecular dynamics simulation is presented in Figure 2, where the heterogeneity of the surface and the large variety of $(SiO)_n$ cycles ($n = 3-7$) are clearly apparent. One can also notice the presence of several types of silanol groups: (i) geminal silanol groups located on the same silicon atom, (ii) vicinal silanol groups bonded through a siloxane bridge, and (iii) adjacent silanol groups connected by two consecutive siloxane bridges (Figure 2).

In the present work, a cluster approach is used to model the tridentate amorphous silica support, and the nickel center is used as a probe of its local environment. The cluster models are derived from the $(SiO)_n$ cycles observed in the molecular dynamics picture of amorphous silica (Figure 2). Density functional theory (DFT) calculations are then performed in order to test the ability of each framework model cluster to reproduce the experimental features of previously described silica-supported $Ni^{II}(O)_3$ species (Table 1): (i) the three-coordinated nickel ion of C_{3v} close to D_{3h} symmetry and (ii) the Ni−O bond lengths, in agreement with EXAFS measurements.

Although the cluster approach takes into account only the surface atoms lying close to the metallic center, it has the advantage to allow high-level calculations (ab initio or DFT) that are expected to yield a precise local picture of the studied site. Cluster models were successfully used to study the nature of titanium active sites in titanosilicate catalysts,[22] to model CO or CD_3CN adsorption on Lewis sites of MgO,[23,24] or to investigate the interaction of Ni, Pd, and Pt on the same support.[25] The cluster approach was also extensively used to model acidic sites,[26] CO and NO,[27] or hydrocarbon[28] adsorption in zeolites. The reliability of small-cluster models was demonstrated in the case of Cu-exchanged zeolites.[29] A similar approach is indeed used by experimentalists when model compounds of the supported active site of heterogeneous catalysts are synthesized and characterized in order to reproduce the properties of the active site in the bulk.[30] For example, silasesquioxanes and metallasilasesquioxanes can provide molecular-level insights into the surface chemistry of silica and silica-supported transition-metal catalysts.[31−33] The originality of our approach is that it deals with a real amorphous surface and not with models systems which can be crystalline materials such as the above-mentioned β-cristobalite, zeolites, bulk oxides with simple structures such as MgO, or molecular models such as silsesquioxanes. Despite their interest per se, their use to represent the amorphous silica surface however cannot overcome the "material gap" since they are crystalline or molecularly well-defined.

Computational Details

Geometries were fully optimized using the GAUSSIAN94 program package[34] within the framework of DFT at the B3PW91 level using a 6-31G** basis except for Ni, for which the DGauss DZVP2 Polarized DFT Orbitals Basis Sets[35] basis were used.

Calculations were conducted at the spin-restricted level in the case of singlet states, whereas triplet states were treated at the spin-restricted open-shell level or spin-unrestricted level.

The SCF density tolerance was set to 10^{-5} e/bohr^3 when convergence with the standard value was not possible, especially on the large framework models. In the latter case, owing to the inordinate flatness of potential energy surface, it was impossible

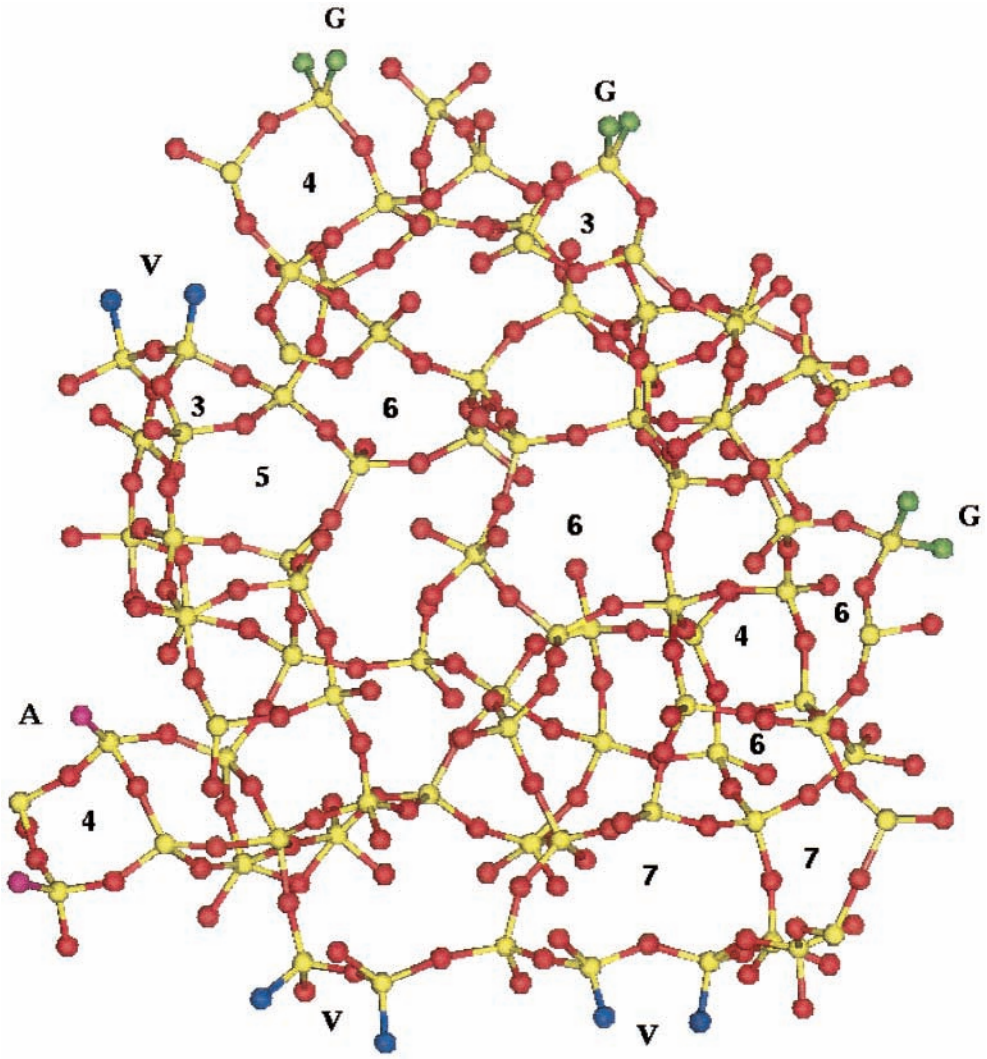

Figure 2. Snapshot of a silica surface obtained by molecular dynamics simulation and generated from librairies within the MSI graphical interface InsightII.[54] H atoms of hydroxyl groups have been omitted for clearness. The variety of surface silanol groups is illustrated: blue (V) = vicinal OH groups, green (G) = geminal OH groups, and violet (A) = adjacent OH groups. Numbers are related to the number of silicon (T) atoms of the ring.

sometimes to unambiguously identify a structure as a true minimum. The optimization procedure was then interrupted when the energy was stable within 10^{-6} hartree.

Choice of the Model Clusters

The model framework clusters used in this work will be referred to using the terminology accepted in zeolite chemistry where the size of the rings is given on the basis of the number of T atoms (T = Si or Al) except oxygen atoms. The model clusters will therefore be referred to as *n*T, depending on the number *n* of Si atoms

$(OH)_2(H_2O)$. The simplest way to model the tridentate silica surface is to use two hydroxyl groups and one water molecule. The resulting $Ni(OH)_2(H_2O)$ model complex may be used to extract qualitative trends. Indeed, we do not expect water and hydroxyl groups to be good models of the silica ligand because of the difference in electron-donating properties, although it was shown that silica lies between OH^- and H_2O in the spectrochemical series: $OH^- < AlO^- < ZO^- < SiO^- < H_2O$, which describes the relative ligand strength of hydroxyle, alumina, zeolite, silica, and water, respectively.[4] Water molecules were also used by Schneider et al.[36] to model Cu-exchanged ZSM-5 zeolites. They found a good agreement between the calculations using water molecules and the ones using a more elaborate model zeolitic framework as long as the coordination environment of the copper ion was realistic enough.[29]

Si_2O_3 (2T). The simplest framework model cluster involving two silicon tetrahedra is $(Si_2O_3H_4)^{2-}$ (Figure 3), which will be referred to as **Si_2O_3** or **2T**. It is made of two vicinal silanolate groups (SiO^-) bonded through an oxygen bridge. The dangling bonds of Si which would actually connect the cluster to the amorphous silica surface are saturated by hydrogens atoms. This cluster has already been used to model acid sites in zeolites.[37,38] The three oxygen atoms of this cluster are able to coordinate the nickel ion, and this model was previously used in our group to describe the silica three-coordinated Ni^{II} and Ni^{I} sites.[8,14]

Si_3O_6 (3T). $(Si_3O_6H_4)^{2-}$ (Figure 3), which will be referred to as **Si_3O_6** or **3T**, is a six-membered ring made of two silanolate and one silanol groups with the silicium atoms bonded through oxygen bridges and terminated by H atoms. The chair conformation of the Si_3O_3 ring was shown to be more stable than the planar one similar to six-carbon rings.[39] The Ni^{II} ion is then bound to both silanolate groups and to the silanol group of this rigid model.

Si_4O_7 (4T). $(Si_4O_7H_6)^{2-}$ (Figure 3), which will be referred to as **Si_4O_7** or **4T**, is an eight-membered ring made of two silanolate and one silanol groups with the silicium atoms bonded through oxygen bridges and terminated by H atoms. The crown

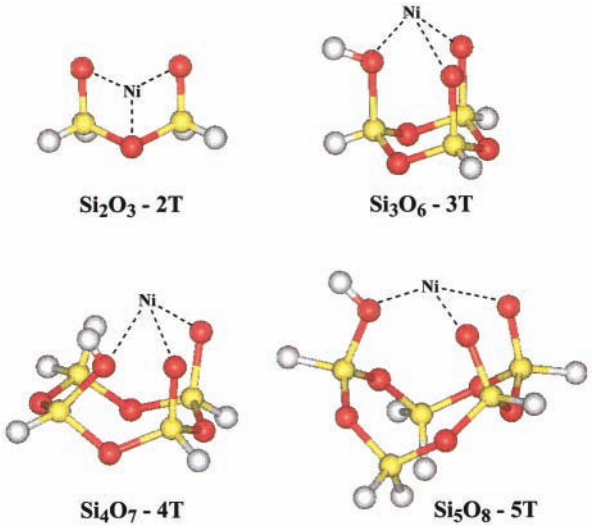

Figure 3. Cluster models of the tridentate amorphous silica surface considered in this work. dotted black lines indicate the expected Ni^{II}−O bonds.

conformation of the Si_4O_4 ring was reported to be more stable than the planar one similar to eight-carbon rings.[39] The Ni^{II} ion is then bound to both silanolate groups and to the silanol group of this model.

Si_5O_8 (5T). $(Si_5O_8H_8)^{2-}$ (Figure 3), which will be referred to as **Si_5O_8** or **5T**, is a 10-membered ring bearing two vicinal silanolate groups in positions 1 and 3 and one isolated silanol group in position 7. This model is very flexible and allows various relative positions of the vicinal and isolated silanol(ate) groups which may coordinate the metallic center.

The above clusters have been tested in their ability to reproduce the experimental structure obtained for three-coordinated silica-supported Ni^{II}_{3c} (Table 1). For each model cluster, the geometry of the corresponding Ni^{II}_{3c} model complex is fully optimized in the singlet and in the triplet electronic state. Moreover, the symmetry of the nickel center and the calculated Ni−O bond lengths are compared with those obtained from EXAFS and diffuse reflectance spectroscopy measurements.

Results and Discussion

Ni Spin State. The energy difference between the lowest triplet (^3F, $3d^84s^2$) and singlet (^1D, $3d^94s^1$) electronic states of the isolated nickel atom is only 3410 cm^{-1} (9.75 kcal/mol).[40,41] However, for the isolated Ni^{II} cation, such a difference is larger: 14032 cm^{-1} (40.12 kcal/mol).[40] The ground triplet state ($^3\Sigma^-$) of the NiO molecule has been extensively studied experimentally[42,43] and theoretically.[44−47] The separation between the triplet state ($^3\Sigma^-$) and the singlet state ($^1\Sigma^+$) depends on the correlation level included in the calculation method and lies in the range of the one of the isolated Ni^{II} cation.[48]

From these findings and the magnetic measurements (Table 1), a triplet spin state is expected for the silica-supported Ni^{II}_{3c} sites. However, the separation between the triplet and singlet spin states is expected to be influenced by both the symmetry and the ligands coordinated to the nickel center. For each model considered hereafter, both singlet and triplet states were therefore considered in order to estimate this energy difference.

$Ni(OH)_2(H_2O)$. The geometry of the model complex $Ni(OH)_2(H_2O)$ has been fully optimized in the triplet and singlet spin state (Table 2). In the less stable singlet state structure, irrelevant hydrogen bonds occur. The triplet state model complex exhibit a C_s symmetry, and Ni−OH distances in good agreement

TABLE 2: Comparison of Selected Bond Lengths (in Å), Angles (in deg), and Mulliken Charges Obtained from Calculations Involving the $(OH)_2H_2O$) Model

	triplet	singlet
Ni−OH (Ni−OH_2)	1.770, 1.771 (2.137)	1.796, 1.732 (1.962)
angles α, β, γ^a	160.1 99.7, 99.8	111.8 167.8, 79.1
$\alpha+\beta+\gamma$	359.6	358.7
Ni−O−H angles	117.6, 117.7 106.0	111.9, 113.2 107.7, 82.8
Ni charge	0.65	0.57
O charge	−0.70, −0.57	−0.60, −0.64, −0.70
total energy (Ha)	−1736.04532	−1736.03042
relative energy	0.0	9.3

[a] α = HO−Ni−OH; β, γ = HO−Ni−OH_2.

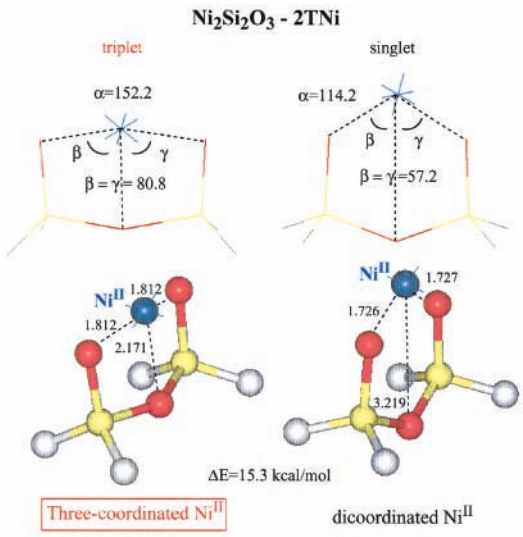

Figure 4. Comparison of the optimized geometries of singlet and triplet state of $Ni^{II}Si_2O_3$. Ni−O distances are in Å and angles in deg.

with the experimental values. It may be considered as the ideal geometry that the nickel center would adopt without steric constraints. The structure exhibits the two following features: (i) a planar environment ($\alpha+\beta+\gamma = 360°$, see Table 2) of nickel of local C_{2v} symmetry and (ii) Ni−O−H angles (corresponding to Ni−O−Si angles in the real complex) of 117°.

$NiSi_2O_3$ (2TNi). The Ni^{II} ion initially equidistant of about 2 Å from the three oxygen atoms moves closer toward the two silanolate groups during the singlet state geometry optimization. The Ni−silanolate distance shortens down to 1.727 Å, whereas the Ni−siloxane distance increases so much that this bond is broken in the optimized structure (Table 3 and Figure 4), yielding a dicoordinated Ni^{II} complex of C_s symmetry. Similar results were obtained by Hass et al.[29] During full optimization of the charged $[CuOSi_2(OH)_6]^+$ cluster model, where Cu^+ is initially bound to the siloxane bridge only, the structure of the cluster is distorted to form Cu−O bonds of 1.9 Å with the in-plane terminal OH groups. Simultaneously, the distance of Cu to bridge oxygen increases to 2.55 Å, yielding an optimized structure analoguous to the one described here for singlet state $Ni^{II}Si_2O_3$. However, the above Ni and Cu cluster models are not strictly related because in one case, the copper cation is attached to a neutral silica surface whereas in the other case, the nickel cation stands formally for the charge compensation of a doubly negatively charged silica surface.

Starting from the same model complex as above, the 3-fold coordination is retained during the triplet state geometry optimization (Table 3 and Figure 4). Spin-restricted open-shell calculations yield results very similar to those of spin-unrestricted calculations. Only the former will be therefore used

TABLE 3: Comparison of Selected Bond Lengths (in Å) and Angles (in deg), and Mulliken Charges Obtained from Calculations Involving the Si_2O_3 (2T) Model[a]

	triplet unrestricted	triplet restricted−open	singlet restricted	$Si_2O_3H_6$ (this work)	$Si_2O(OH)_6$ (ref 39)
		Bond Length			
Ni−O_t	1.812, 1.812	1.813, 1.813	1.727, 1.726		
Ni−O_b	2.171	2.169	3.219		
Si−O_t	1.650	1.650	1.663	1.65−1.67	1.64−1.66
Si−O_b	1.710	1.710	1.658	1.65−1.66	1.65
O−H	−	−	−	0.965	0.97
O−H[b]	−	−	−	2.492	2.52
		Angles			
O_t−Si−O_b	101.2	101.1	109.1, 109.2	110.5, 110.7	107.8−113.7
Si−O_b−Si	148.1	148.1	133.5	132.9	132.1
O_t−Si−H	113.7, 114.2	113.7, 114.2	110.0	105−112	
α	152.2	152.1	114.2		
β, γ[c]	80.8, 80.8	80.8, 80.8	57.2, 57.2		
$\alpha+\beta+\gamma$[b]	313.8	313.7	228.6		
Ni−O_t−Si	95.7, 95.8	95.8	125.6,125.3		
Ni−O_b−Si	82.0	82.1	67.7, 67.9		
		Mulliken Charges			
Ni	0.70	0.70	0.72	−	−
O_t	−0.69	−0.69	−0.69	−0.62, −0.64	−0.82
O_b	−0.70	−0.70	−0.66	−0.65	−0.70
Si	0.93	0.93	0.93	0.88	1.24
total energy (Ha)	−2315.06900	−2315.06773	−2315.04463		
relative energy (kcal/mol)	0.0	0.8	15.3		

[a] O_b and O_t denote bridging and terminal oxygens, respectively. [b] Hydrogen bond. [c] $\alpha = O_t$−Ni−O_t; β, $\gamma = O_b$−Ni−O_t.

hereafter to investigate the triplet state of larger framework cluster models. The Ni−silanolate distance is slightly longer (0.05 Å) than the one measured by EXAFS, whereas the Ni−siloxane distance is 0.1 Å longer than the experimental one. The sum of the valence angles of Ni (i.e., 314°) suggests a large deviation from the D_{3h} symmetry. Both latter findings desagree with the experimental description. Moreover, the Ni−O−Si angles deviate substantially from the ideal value of 117° suggested above by the $(OH)_2(H_2O)$ model.

The geometry of the free neutral framework cluster $Si_2O_3H_6$ has been optimized at the same calculation level and compared to the one calculated by Pereira et al.[39] for $Si_2O(OH)_6$ at the BLYP level using a numerical triple-ζ basis. Both structures are very similar considering bond lengths and angles (Table 3). The singlet state $Ni^{II}{}_{2c}$ complex occurs almost without framework alteration; however, in the triplet state Ni^{II} complex, the coordination to the support is accompanied by Si−O_b bond elongation and opening of the Si−O_b−Si angles (Table 3).

$NiSi_3O_6$ (3TNi). The Ni^{II} ion initially equidistant of about 2 Å from the three oxygen atoms moves closer toward the two silanolate groups during the singlet state geometry optimization. The Ni−silanolate distance shortens down to 1.781 Å, whereas the Ni−siloxane distance increases up to 2.130 Å (Table 4), yielding a three-coordinated Ni^{II} complex of symmetry close to D_{3h}.

The triplet state geometry optimization yields a Ni^{II} complex where the Ni−silanolate distance lies now out of the range of the EXAFS measurements by 0.1 Å, whereas the Ni−siloxane distance is in agreement with the experimental measurements (Table 4 and Figure 5). The sum of the valence angles of Ni has increased up to 323° suggesting that the symmetry is C_{3v} but has moved closer to D_{3h} in comparison to the previous $Ni^{II}{}_{3c}$-Si_2O_3 model. The Ni−O−Si angles still deviate substantially from the ideal value of 117° suggested by the $(OH)_2(H_2O)$ model.

The optimized geometry of the corresponding neutral framework cluster model $Si_3O_6H_6$ has been compared to the one calculated by Pereira et al.[39] for $Si_3O_3(OH)_6$ (Table 4). In

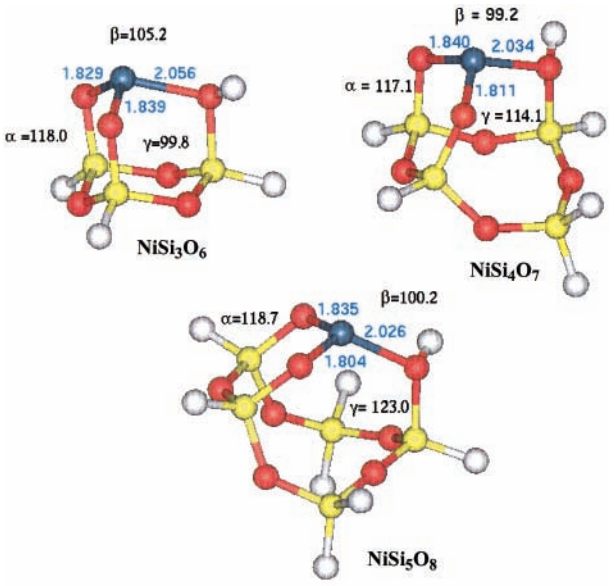

Figure 5. Comparison of the optimized geometries of triplet states of $Ni^{II}Si_3O_6$, $Ni^{II}Si_4O_7$, and $Ni^{II}Si_5O_8$. Ni−O distances are in Å and angles in deg.

contrast to the chair conformation of the Si_3O_3 ring in the nickel model complex, a planar ring conformation already reported[39] for $Si_3O_3(OH)_6$ is obtained. However, this structure is expected to be less stable by 6 kcal/mol than the ring chair conformation, where the axial hydroxyl groups are involved in three hydrogen bonds.[39]

Upon nickel coordination, the Si−O_b−Si angles shorten and the Si−O_b bonds are elongated as compared to the free more stable cluster. The Si−OH bond length increases significantly from 1.64 up to 1.74 Å.

$NiSi_4O_7$ (4TNi). The Ni^{II} ion initially equidistant of about 2 Å from the three oxygen atoms moves closer toward the two silanolate groups during the singlet state geometry optimization. The Ni−silanolate distance shortens down to 1.78 Å, whereas

TABLE 4: Comparison of Selected Bond Lengths (in Å), Angles (in deg), and Mulliken Charges Obtained from Calculations Involving the 3T Model[a]

	triplet	singlet	$Si_3O_3(OH)_3H_3$ (this work)	$Si_3O_3(OH)_6$ planar[39]	$Si_3O_3(OH)_6$ chair[39]
		Bond Length			
Ni−O	1.829, 1.839	1.781, 1.782			
Ni−OHSi	2.056	2.130			
Si−O_t (Si−OH)	1.631,1.633, (1.743)	1.643, 1.646, (1.726)	(1.64−1.65)	(1.64)	(1.64−1.68)
Si−O_b	1.63−1.70	1.64−1.71	1.65−1.66	1.64−1.65	1.67−1.68
O−H	0.968	0.966	0.962	0.98	0.98−0.99
O−H[b]	none	none	none	none	2.69−2.81
		Angles			
O_t−Si−O_b	103.8−110.6	104.9−110.1	106−112		
Si−O_b−Si	117.4−121.1	115.2−123.6	131−134	130.7−132.9	121.3−122.4
O_b−Si−O_b	103.8, 103.9, 111.9	104.0, 104.0, 110.9	106.2, 106.2, 108.7	106.7−101.8	107.2−108.2
O_t−Si−H (O_t−Si−O_t)	114.4, 114.4, 108.2	108.9−113.1	106−112	(105.2)	(110.1−110.8)
Si−O−H	112.1	115.2	117−118	111.2−114.8	109.8−112.2
α	118.0	104.2			
β, γ[c]	105.2, 99.8	100.3, 127.5			
$\alpha+\beta+\gamma$[c]	323.0	332.0			
Ni−O_t−Si	106.9, 108.1	101.6, 110.4			
Ni−(OH)−Si	106.0	96.2			
		Mulliken Charges			
Ni	0.67	0.58			
O_t	−0.69, −0.66	−0.65, −0.66			
O_b	−0.66, −0.67	−0.66, −0.67			
total energy (Ha)	−2830.36385	−2830.32537			
relative energy (kcal/mol)	0.0	24.2		−6.1	0.0

[a] O_b and O_t denote bridging and terminal oxygens, respectively. [b] Hydrogen bond. [c] α = O−Ni−O; β, γ = HO−Ni−O.

TABLE 5: Comparison of Selected Bond Lengths (in Å), Angles (in deg), and Mulliken Charges Obtained from Calculations Involving the Si_4O_7 Model[a]

	triplet	singlet	$Si_4O_4(OH)_3H_5$ (this work)	$Si_4O_4(OH)_8$ planar[39]	$Si_4O_4(OH)_8$ crown[39]
		Bond Length			
Ni−O	1.840, 1.811	1.776, 1.796			
Ni−OHSi	2.034	1.978			
Si−O_t (Si−OH)	1.630, 1.639, (1.739)	1.641, 1.644, (1.743)	(1.651, 1.648, 1.648)	(1.64)	(1.62−1.66)
Si−O_b	1.62−1.70	1.63−1.68	1.63−65	1.62	1.64−1.65
O−H	0.967	0.970	0.961	0.98	0.98−1.03
O−H[b]	none	none	none	none	1.61−1.62
		Angles			
O_t−Si−O_b	105−111	104−111	105−110		
Si−O_b−Si	131−133, 151	124.2−136.6	144−152	160.4	125.8−126.3
O_b−Si−O_b	107−115	107−114	111−112	109.5	111.2−112.2
O_t−Si−H (O_t−Si−O_t)	105.9−114.3	108−113	111−112	(106.0)	(113.2−114.8)
Si−O−H	111.9	112.4	116−117	112.2−114.5	106.2−114.3
α	117.1	161.4			
β, γ[c]	99.2, 114.2	99.8, 88.0			
$\alpha+\beta+\gamma$[c]	330.5	349.2			
Ni−O_t−Si	105.5, 118.3	107.6, 106.0			
Ni−(OH)−Si	110.4	103.0			
		Mulliken Charges			
Ni	0.67	0.48	−		
O_t	−0.68, −0.72	−0.66, −0.65	−0.62, −0.61		
O_b	−0.64, −0.66	−0.66	−0.63		
total energy (Ha)	−3196.30676	−3196.28028	−1689.46948		
relative energy (kcal/mol)	0.0	16.6		−31.9	0.0

[a] O_b and O_t denote bridging and terminal oxygens, respectively. [b] Hydrogen bond. [c] α = O−Ni−O; β, γ = HO−Ni−O.

the Ni−siloxane distance decreases to 1.978 Å (Table 5), yielding a three-coordinated Ni^{II} complex of D_{3h} symmetry whose geometry is very similar to the experimental one.

In the triplet state optimized geometry, the Ni−silanolate distance is now out of the range of the EXAFS measurements by 0.1 Å, whereas the Ni−siloxane distance is in agreement with the experimental measurements (Table 5 and Figure 5). The sum of the valence angles of Ni has again increased as compared to those of the above Si_3O_6 model, suggesting that the symmetry has moved further toward D_{3h}. The Ni−O−Si angles are now closer to the ideal value of 117° suggested above by the $(OH)_2(H_2O)$ model.

In contrast to the crown conformation of the Si_4O_4 ring observed in the above nickel model complex, a planar ring conformation already reported[39] for $Si_3O_3(OH)_6$ is obtained in the optimized geometry of the neutral framework cluster model $Si_4O_7H_8$ (Table 5). However, this structure is expected to be less stable by 32 kcal/mol than the crown conformation, where the hydroxyl groups are involved in a cyclic system of four hydrogen bonds.[39]

TABLE 6: Comparison of Selected Bond Lengths (in Å), Angles (in deg), and Mulliken Charges Obtained from Calculations Involving the Si_5O_8 (5T) Model

	triplet	singlet
Ni−O distance	1.804, 1.835	1.794 1.766
Ni−OH distance	2.026	1.953
α, β, γ^a	118.7, 100.2, 123.0	88.8, 164.8, 103.9
$\alpha + \beta + \gamma^a$	341.9	357.5
Ni−O_t-Si	116.8, 115.4	118.5, 110.3
Ni−(OH)-Si	117.6	109.6
	Mulliken Charges	
Ni	0.71	0.61
O silanolate	−0.72	−0.69
		−0.68
O silanol	−0.67	−0.66
total energy (Ha)	−3562.24389	−3562.22443
relative energy (kcal/mol)	0.0	12.2

[a] α = O−Ni−O; β, γ = HO−Ni−O.

Upon nickel coordination, the Si−O_b−Si angles lie between the corresponding angles observed in the crown and planar conformations of the free framework cluster. As already observed above, the Si−OH bond length increases significantly from 1.65 up to 1.74 Å.

$NiSi_5O_8$ (5TNi). The same tendencies noted for the two latter models are confirmed. The singlet state geometry optimization yield a model structure in very good agreement with the experimental measurements. However, a more stable structure (by 12 kcal/mol) results from the triplet state geometry optimization. The Ni−O distances are in the range of the EXAFS measurements (Table 6 and Figure 5). The sum of the valence angles of Ni increased up to 342°, suggesting that the symmetry is closer to D_{3h} than for both previous models. The Ni−O−Si angles are very close to the ideal value of 117° suggested above by the $(OH)_2(H_2O)$ model.

The structural features of the framework are very similar to the one described previously for the Si_4O_7 model.

Among the model clusters investigated here, 5T is therefore the one that reproduces the experimental structure the best (Table 7) in terms of Ni−O bond length and in terms of local nickel symmetry as well. Moreover, it is the model that yields the nickel environment closest to the ideal one suggested above by the $(OH)_2(H_2O)$ model.

The four framework cluster models investigated in this work may be compared in terms of:
(i) model geometry that may favor or hinder frontier orbital overlaps between the oxygen ligands and the metallic center,
(ii) model rigidity that may hinder the accommodation of a three-coordinated Ni^{II}, and
(iii) the effect on the electronic and spin state of the nickel center.

Influence of the Model Cluster on the Frontier Orbital Overlap and Energy Levels. The frontier bonding orbitals have been compared for the models, and no significant difference in the overlap was apparent. Similarly, the energy levels of the frontier orbitals are almost the same, whatever the model cluster considered (Table 8). There is a slight energy shift of the energy levels of *n*T toward the energy levels of the ideal $Ni(OH)_2(H_2O)$ model as *n* increases from 2 to 5. However, the better fit of 5TNi with the experimental results may not be explained on this basis.

Comparaison of the Rigidity of the Various Model Clusters Investigated in This Work. The simplest model complex $Ni(OH)_2(H_2O)$ pictures the ideal nickel environment in the absence of steric requirements of the oxygen ligands. Therefore, the best cluster model of the support is expected to be the one that would allow both a planar environment of the nickel center and Ni−O−Si angles close to 117°. From this point of view, 5T appears as the best probably because of its flexibility.

To evaluate the steric constraint resulting from the nickel coordination, the energy corresponding to the relaxation of the neutral cluster from its geometry in the nickel model complex has been calculated. Silanolates have been replaced by silanol groups in these calculations in order to eliminate electrostatic repulsions and final structures without hydrogen bonds were favored. The relaxation energies are compared in Table 9. Similar relaxation energies are found for singlet and triplet spin states. The relaxation energy is minimum for the 5T model suggesting that rigidity or steric factors are determinant factors in the coordination of Ni^{II}. The conformational flexibility of Si_5O_8 is expected to allow various relative positions of the three oxygen ligands to Ni^{II}. The latter is allowed to be located close to the plane formed by the oxygen atoms.

Influence of the Model Cluster on the Electronic and Spin State of Nickel. The deposition of Ni° onto amorphous silica is difficult to study experimentally because of the desordered nature of the support. Moreover, nickel atoms do not remain isolated. There is nucleation and growth of nickel particles by migration of metallic nickel onto the support. These two steps have been evidenced and used to prepare metallic nickel particles of controlled size.[49] EHMO calculations have shown that the nucleation sites are preferably extraframework ions in high oxidation state.[50] This work focuses on these potential nucleation sites, i.e., isolated Ni^{II} cations, supported on silica that may be subsequently reduced into Ni^{I} (for which the coordination mode of the support is under theoretical investigation by comparaison to the experimental characterization[10,15]) and finally to metallic nickel.

As expected from the known energy difference between the lowest triplet and singlet electronic states of isolated nickel atoms and Ni(II) ions, the calculated triplet state Ni(II) complex is always more stable than the corresponding singlet state Ni(II) complex, whatever the framework cluster model. However, the energy difference between both spin states depends on the cluster model and is lower for the best model complexes such as $Ni(OH)_2(H_2O)$ and 5TNi (9.3 and 12 kcal/mol, respectively). The triplet and singlet spin states respectively correspond to the 3-fold and 2-fold coordinations of the Ni center. This suggests that the coordination of Ni^{II} to the silanol group is weak (in agreement with the longer Ni−O bond length calculated or measured by EXAFS) and may be easily broken by a small external perturbation such as the approach of a ligand from the gas phase for example, yielding a di-coordination with

TABLE 7: Comparison of the Ni−O Distances (Å) and of the Sum of the Valence Angles (deg) around Ni (Triplet Spin State) for the Various Cluster Models Investigated in This Work

	$Ni(OH)_2(H_2O)$	2TNi	3TNi	4TNi	5TNi
Ni−silanolate	1.770, 1.771	1.812, 1.812	1.829, 1.839	1.840, 1.811	1.804, 1.835
Ni−silanol (Ni−siloxane)	2.137	2.171	2.056	2.034	2.026
Σ valence angles of Ni	359.6	313.8	323.0	330.5	341.9

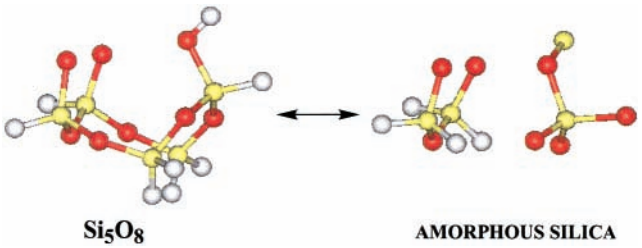

Figure 6. Correspondence of the Si_5O_8 framework model cluster on the real silica support.

TABLE 8: Energy Levels at the Fermi Level (in hartrees) for the Various Ni Complexes Calculated at the ROB3PW91/6-31G/DZVP2(Ni) Level in the Triplet State**

	$Ni(OH)_2(H_2O)$	2TNi	3TNi	4TNi	5TNi
LUMO	+0.00342	−0.03285	−0.05023	−0.04535	−0.03411
HOMO	−0.12142	−0.15983	−0.14992	−0.14744	−0.14639
HOMO-1	−0.12612	−0.16262	−0.15901	−0.15893	−0.16003
HOMO-2	−0.26396	−0.29780	−0.28548	−0.28037	−0.27545
HOMO-3	−0.26600	−0.29969	−0.29058	−0.29207	−0.29387
HOMO-4	−0.27791	−0.33004	−0.32076	−0.31086	−0.30610

TABLE 9: Relaxation Energies of Various Models in Kcal/Mol

	relaxation energy singlet state	relaxation energy triplet state	relaxation energy difference
$Si_2O_3H_6$	29.0	33.6	4.6
$Si_3O_6H_6$	42.8	41.3	−1.5
$Si_4O_7H_8$	nc[a]	28.4	nc[a]
$Si_5O_8H_{10}$	nc[a]	30.7	nc[a]

[a] nc = not calculated.

TABLE 10: Mulliken Charges and Spin Densities of the Nickel Center in the Various Ni Complexes Calculated at the B3PW91/6-31G/DZVP2(Ni) Level in the Triplet State**

	$Ni(OH)_2(H_2O)$	2TNi	3TNi	4TNi	5TNi
Ni spin density	1.61	1.61	1.62	1.62	1.63
Ni charge	0.65	0.70	0.67	0.67	0.71
OH, O_t or silanolate charge	−0.70 (**O**H)	−0.69 (O_t)	−0.69	−0.72	−0.72
H_2**O**, O_b or silanol charge	−0.57 (H_2**O**)	−0.70 (O_b)	−0.66	−0.68	−0.67

the support in agreement with the high reactivity of the Ni^{II}_{3c} sites observed experimentally.

In the more stable triplet-state model nickel complexes, the Mulliken spin density is always concentrated mostly on the nickel center (Table 10), whatever the framework cluster model used. Small contributions are observed on the oxygen ligands of the support. The nephelauxetic effect appears therefore to be low probably because Ni^{II} and O^{2-} are hard in the Pearson's hardness scale.[51] However, the Mulliken charge calculated for Ni^{II} is lower than +1, suggesting that there is a substantial charge transfer from the support to the nickel ion (Table 10) and that the Ni−O bond is not completely ionic in nature. This charge transfer is very similar, whatever the model cluster used (Table 10).

In conclusion, among the model clusters investigated in this work, 5T, because of its flexibility, is the one that best reproduces the experimental results. Such a flexibility is known to exist in the amorphous silica surface or in zeolites.[52] This model may be assimilated with two vicinal silanolates and one neighboring isolated silanol or siloxane bridge on the real silica surface (Figure 6). The low probability of finding three OH groups per 5T ring suggests that the dative bond involves preferably the oxygen of a siloxane bridge. Moreover, the involvement of an isolated silanol or siloxane bridge belonging to a neighboring 6T ring cannot be excluded. Indeed 6T rings appear to be more likely than 5T rings from the molecular dynamics simulation (Figure 2).

Conclusion

In this work, various framework model clusters have been investigated in order to model the tridentate amorphous silica ligand using the Ni^{II} ion as a probe. The originality of our approach is that it deals with the real amorphous surface and not with models systems which can be crystalline materials such as β-cristobalite, zeolites, bulk oxides with simple structures such as MgO, or molecular models such as silsesquioxanes. Despite the interest per se of the latter, their use to represent the amorphous silica surface, however, cannot overcome the " material gap " since they are crystalline or molecularly well-defined.

The various nT ($n = 2-5$) models allow to predict three-coordination for Ni^{II} ions, but 5T is the one that reproduces best the experimental symmetry (C_{3v} close to D_{3h}) and the Ni−O distances measured by EXAFS. Because of its flexibility, the latter cluster model is able to accommodate Ni^{II} ions in almost D_{3h} symmetry with the lowest constraint. It may be assimilated to two vicinal silanolates and one neighboring isolated silanol or siloxane bridge of the real silica surface.

Modeling has been used here as an analysis tool to complement the other experimental characterization techniques. It allowed us to refine our previous concept of the tridentate ligand nature of the silica support. In this work, the adsorption site has been investigated in details, and the resulting structure will now facilitate the modeling of the complexes obtained by adsorption of ligands of the gas phase or by interaction with reactants or products such as for example benzene[53] during the catalytic cyclotrimerization of acetylene. The Ni^{II} ions studied here are the precursors of Ni^{I} ions active as olefin oligomerization catalysts. The results obtained here for Ni^{II} ions set therefore the basis for the study of their reduced analogues.

This study suggests the existence on the silica support of particular cycles that would be able to selectively interact with nickel ions.The nickel deposition onto the support may therefore be driven by molecular recognition and this will be reported on in future work.

Acknowledgment. The authors would like to thank Luc-Henri Jolly for computational assistance, IDRIS (Institut du Développement et des Ressources en Informatique Scientifique, Orsay, France) for computing facilities, Ministère de la Recherche for financial support and Dr. Maggy Kermarec for helpful discussions.

References and Notes

(1) Gates, B. C. *Chem. Rev.* **1995**, *95*, 511.
(2) Goodman, D. W. *Chem. Rev.* **1995**, *95*, 523.
(3) (a) Che, M. *Stud. Surf. Sci. Catal.* **1993**, *75A*, 31. (b) Che, M. *Stud. Surf. Sci. Catal.* **2000**, *130A*, 115.
(4) Lepetit, C.; Che, M. *J. Mol. Catal.* **1995**, *100*, 147.
(5) Dyrek, K.; Che, M. *Chem. Rev.* **1997**, *97*, 305.
(6) Lepetit, C.; Kermarec, M.; Olivier, D. *J. Mol. Catal.* **1989**, *51*, 95.
(7) Lambert, J.-F.; Hoogland, M.; Che, M. *J. Phys. Chem. B* **1997**, *101*, 10347.
(8) Olivier, D.; Bonneviot, L.; Cai, F. X.; Che, M.; Gihr, P.; Kermarec, M.; Lepetit-Pourcelot, C.; Morin, B. *Bull. Soc. Chim. Fr.* **1985**, *3*, 370.
(9) Bonneviot, L.; Legendre, O.; Kermarec, M.; Olivier, D.; Che, M. *J. Colloid Interface Sci.* **1990**, *134*, 534.
(10) Lepetit, C.; Kermarec, M.; Olivier, D. *J. Mol. Catal.* **1989**, *51*, 73.
(11) Carriat, J. Y.; Lepetit, C.; Kermarec, M.; Che, M. *J. Phys. Chem. B* **1998**, *102*, 3742.
(12) Carriat, J. Y. Thesis, University Pierre and Marie Curie, Paris, France, 1996.

(13) Carriat, J. Y.; Che, M.; Kermarec, M.; Verdaguer, M.; Michalowicz, A. *J. Am. Chem. Soc*. **1998**, *120*, 2059.
(14) Bonneviot, L.; Cai, F. X.; Che, M.; Kermarec, M.; Legendre, O.; Lepetit, C.; Olivier, D. *J. Phys. Chem.* **1987**, *91*, 5912.
(15) Cai, F. X.; Lepetit, C.; Kermarec, M.; Olivier, D. *J. Mol. Catal.* **1987**, *43*, 93.
(16) Krejei, I.; Ott, E. *J. Phys. Chem.* **1931**, *35*, 2061.
(17) Iler, R. K. *The Colloid Chemistry of Silicates*; Cornell University Press: Ithaca, NY, **1955**, 242.
(18) Hsu, L. Y.; Shore, S. G.; D'Ornelas, L.; Choplin, A.; Basset, J. M. *J. Catal*. **1994**, *149*, 159.
(19) Shay, T. B.; Hsu, L. Y.; Basset, J. M.; Shore, S. G. *J. Mol. Catal*. **1994**, *86*, 501.
(20) Garofalini, S. H. *J. Non-crystalline Solids* **1990**, *120*, 1.
(21) Feuston, B. P.; Garofalini, S. H. *J. Chem. Phys.* **1989**, *91*, 564.
(22) Sinclair, P. E.; Sankar, G.; Catlow, C. R. A.; Thomas, J. M.; Maschmeyer, T. *J. Phys. Chem. B* **1997**, *101*, 4232.
(23) Pelmenschikov, A. G.; Morosi, G.; Gamba, A.; Coluccia, S. *J. Phys. Chem.* **1995**, *99*, 15018.
(24) Pelmenschikov, A. G.; Morosi, G.; Gamba, A.; Coluccia, S.; Martra, G.; Paukshtis, E. A. *J. Phys. Chem.* **1996**, *100*, 5011.
(25) Lopez, N.; Illas, F. *J. Phys. Chem. B* **1998**, *102*, 1430.
(26) Gale, J. D.; Catlow, C. R. A.; Carruthers, J. R. *Chem. Phys. Lett.* **1993**, *216*, 155.
(27) Zhanpeisov, N. U.; Nakatsuji, H.; Hada, M.; Nakai, H.; Anpo, M. *Catal. Lett.* **1996**, 173.
(28) Sauer, J.; Ugliengo, P.; Garrone, E.; Saunders, V. R. *Chem. Rev.* **1994**, *94*, 2095.
(29) Hass, K. C.; Schneider, W. F. *J. Phys. Chem.* **1996**, *100*, 9292.
(30) Piquemal, J. Y.; Bois, C.; Brégeault, J. M. *Chem. Commun.* **1997**, 473.
(31) Feher, F. J.; Budzichowski, T. A. *Polyhedron* **1995**, *14*, 3239.
(32) Maschmeyer, T.; Klunduk, M. C.; Martin, C. M.; Shephard, D. S.; Thomas, J. M.; Johnson, B. F. G. *Chem. Commun.* **1997**, 1847.
(33) Maschmeyer, T.; Thomas, J. M.; Masters, A. F. In *New Trends in Materials Chemistry*; Catlow, R., Cheetham, A. Eds.; NATO ASI Series C; Kluwer: Norwell, MA, 1997; Vol. 498, p 461.
(34) Frisch, M. J.; Trucks, G. W.; Schlegel, H. B.; Gill, P. M. W.; Johnson, B. G.; Robb, M. A.; Cheeseman, J. R.; Keith, T.; Petersson, G. A.; Montgomery, J. A.; Raghavachari, K.; Al-Laham, M. A.; Zakrzewski, V. G.; Ortiz, J. V.; Foresman, J. B.; Cioslowski, J.; Stefanov, B. B.; Nanayakkara, A.; Challacombe, M.; Peng, C. Y.; Ayala, P. Y.; Chen, W.; Wong, M. W.; Andres, J. L.; Replogle, E. S.; Gomperts, R.; Martin, R. L.; Fox, D. J.; Binkley, J. S.; Defrees, D. J.; Baker, J.; Stewart, J. P.; Head-Gordon, M.; Gonzalez, C.; Pople, J. A. *Gaussian 94*, revision E.2; Gaussian, Inc.: Pittsburgh, PA, 1995.
(35) Godbout, N.; Salahub, D. R.; Andzelm, J.; Wimmer, E. *Can. J. Chem*. **1992**, *70*, 560.
(36) Schneider, W. F.; Hass, K. C.; Ramprasad, R.; Adams, J. B. *J. Phys. Chem.* **1996**, *100*, 6032.
(37) Allavena, M.; Kassab, E.; Evleth, E. *J. Mol. Struct.* **1994**, *325*, 85.
(38) Teunissen, H. E.; Jansen, A. P. J.; Van Santen, R. A. *J. Phys. Chem.* **1994**, *99*, 5865.
(39) Pereira, J. C. G.; Catlow, C. R. A.; Price, G. D. *J. Phys. Chem. A* **1999**, *103*, 3252.
(40) Moore, C. E. *Atomic Energy Levels*; National Bureau of Standards: Washington, DC, 1971; Vol. III.
(41) Sugar, J.; Corliss, C. *J. Phys. Chem. Ref. Data*, **1985**, *14*, Suppl. No. 2.
(42) Srdanov, V. I.; Harris, D. O. *J. Chem. Phys*. **1988**, *89*, 2748.
(43) Watson, L. R.; Thiem, T. L.; Dressler, R. A.; Salter, R. H.; Murad, E. *J. Phys. Chem.* **1993**, *97*, 5577.
(44) Walch, S. P.; Goddard, W. A., III. *J. Am. Chem. Soc.* **1978**, *100*, 1338.
(45) Castejon, H.; Hernandez, A. J.; Ruette, F. *J. Phys. Chem.* **1988**, *92*, 4970.
(46) Doll, K.; Dolg, M.; Fulde, P.; Stoll, H. *Phys. Rev. B* **1997**, *55*, 10282.
(47) Bauschlicher, C. W.; Maitre, P. *Theor. Chim. Acta* **1995**, *90*, 189.
(48) Bauschlicher, C. W.; Nelin, C. J.; Bagus, P. S. *J. Chem. Phys*. **1985**, *82*, 3265.
(49) Che, M.; Cheng, Z. X.; Louis, C. *J. Am. Chem. Soc*. **1995**, *117*, 2008.
(50) Che, M.; Masure, D.; Chaquin, P. *J. Phys. Chem.* **1993**, *97*, 9022.
(51) Pearson, R. G. *Inorg. Chem.* **1988**, *27*, 734.
(52) Rabo, J. A.; Gadja, G. J. *Catal. Rev.—Sci. Eng.* **1989**−**90**, *31*, 385.
(53) Chaquin, P.; Costa, D.; Lepetit, C.; Che, M. *J. Phys. Chem. A* **2001**, *105*, 4541.
(54) *InsightII 4.0.0*; Molecular Simulations Inc.: Cambridge, 1995.